Human microcephaly ASPM protein is a spindle pole-focusing factor

Ami Ito, Elsa A. Tungadi, Tomomi Kiyomitsu, and Gohta Goshima†

Division of Biological Science, Graduate School of Science, Nagoya University, Furo-cho, Chikusa-ku, Nagoya 464-8602, Japan
†E-mail: goshima@bio.nagoya-u.ac.jp Phone: +81-52-788-6175

Nonsense mutations in the *ASPM* gene have been most frequently identified among familial microcephaly patients. Depletion of ASPM causes spindle pole unfocusing during mitosis in multiple cell types of *Drosophila*. However, it remains unknown whether human ASPM has a similar function. Here, using CRISPR-based gene knockout (KO) and RNA interference combined with chemical inhibitors and auxin-inducible degron, we show that ASPM functions in spindle pole organisation redundantly with the centrosomes and the kinesin-14 motor HSET in human tissue culture cells. Deletion of the *ASPM* gene alone did not affect spindle morphology or mitotic progression. However, when CDK5RAP2, the activator of centrosomal microtubule nucleation, was degraded in *ASPM* KO cells, the spindle poles were unfocused and mitosis was significantly delayed. HSET inhibition in *ASPM* KO cells also resulted in synthetic pole disorganisation. Similarly, a hypomorphic mutation identified in microcephaly patients caused spindle pole unfocusing in the absence of CDK5RAP2, suggesting this spindle pole defect as a possible cause of microcephaly.

Introduction

The most common cause of autosomal recessive primary microcephaly is a homozygous mutation of the *ASPM* gene (Abdel-Hamid et al., 2016; Bond et al., 2002; Bond et al., 2003; Tan et al., 2014). ASPM was originally identified in *Drosophila*, as the orthologue Asp, whose mutation results in abnormal spindle formation (Ripoll et al., 1985). In the absence of Asp, the centrosomes are detached from the main body of the spindle, and spindle microtubules (MTs) are unfocused at the pole (Ito and Goshima, 2015; Morales-Mulia and Scholey, 2005; Saunders et al., 1997; Schoborg et al., 2015; Wakefield et al., 2001). Asp is concentrated at the spindle pole, the area enriched with the spindle MT minus ends. The current model is that Asp binds directly to the spindle MT ends using the middle region containing calponin homology domains and cross-links them each other, thus postulating Asp as a critical pole-focusing factor (Ito and Goshima, 2015). Recent studies have also shown that *asp* mutant flies have reduced brain size (Rujano et al., 2013; Schoborg et al., 2015), which was at least partly attributed to chromosome mis-segregation associated with unfocused spindle poles (Rujano et al., 2013).

The cellular function of human ASPM has been evaluated using RNA interference (RNAi)-mediated knockdown. Small interfering RNA (siRNA)-based knockdown in U2OS cells led to spindle misorientation, cytokinesis failure, reduction in mitotic cells, and apoptosis (Higgins et al., 2010), possibly through interacting with the citron kinase (Gai et al., 2016; Paramasivam et al., 2007). Another study observed downregulation of BRCA1 protein upon ASPM knockdown (Zhong et al., 2005). To the best of our knowledge, the pole-focusing defect commonly observed upon Asp depletion in *Drosophila* has not been reported in studies of human ASPM knockdown. However, RNAi has a general limitation in that the residual protein expression might suffice to fulfil the function of the target protein. Moreover, none of the previous RNAi studies of ASPM involved a rescue experiment in which full-length ASPM was ectopically expressed after endogenous ASPM depletion, leaving the possibility that some of the observed phenotypes were derived from off-target effects of the siRNAs utilised. The effect of mutations identified in microcephaly patients has also not been assessed using a cell culture model. Nevertheless, the lack of the spindle pole phenotype is surprising, given the result obtained in *Drosophila*.

In this study, we used CRISPR/Cas9-based knockout (KO) as well as RNAi to decipher the mitotic function of ASPM in the human HCT116 cell line. Our data provide the first demonstration that human ASPM is an important factor in spindle pole organisation, working redundantly with a centrosomal protein and kinesin-14. Furthermore, mutations identified in microcephaly patients similarly impair this function of ASPM.

Results

No mitotic abnormality upon *ASPM* KO in the human HCT116 cell line

To precisely assess the function of human ASPM, we aimed to delete the *ASPM* gene in HCT116 cells using CRISPR/Cas9-based genome editing. Since it was reported that all ASPM isoforms are translated from a common start codon in exon 1 (Kouprina et

al., 2005), we selected homozygous KO lines by inserting a drug-resistant marker in exon 1 and deleting the start codon (Fig. 1A, B). Immunofluorescence microscopy using anti-ASPM antibody indicated that ASPM was significantly depleted in the selected lines, confirming successful editing (Fig. 1C). However, in a late stage of this project, we noticed that some residual protein expression was still detected with this antibody when the image contrast was further enhanced (Fig. S1A). Therefore, we also selected the cell lines in which the entire open reading frame was replaced by a marker gene cassette (Fig. S1B, C). The polar staining completely disappeared in the complete KO line (KO^{C}; Fig. S1D). In either KO line, we did not observe abnormality in mitotic spindle formation and mitotic progression in time-lapse microscopy of the MTs, suggesting that *ASPM* is not an essential gene for mitosis in this cell line (Fig. 1D, E; Fig. S1E, F; and Movie 1).

Spindle poles were abnormally split upon double inhibition of ASPM and HSET

In addition to *Drosophila* Asp, several factors have been identified to play a role in spindle MT focusing, such as motor proteins (dynein and kinesin-14) and the MT minus-end-localised protein NuMA (Gaglio et al., 1996; Goshima et al., 2005; Hatsumi and Endow, 1992; Manning and Compton, 2007; Merdes et al., 2000; Walczak et al., 1998). The relative contribution of these factors appears to vary depending on the cell type. A previous study in *Drosophila* S2 cells showed that spindle MT focusing at the pole was ensured by the independent actions of kinesin-14 and Asp (Ito and Goshima, 2015). Therefore, we hypothesised that ASPM function may be critical when kinesin-14 activity is suppressed in HCT116 cells.

To test this hypothesis, we treated control and *ASPM* KO cells with CW069, an inhibitor of human kinesin-14 HSET (Watts et al., 2013), and MG132, a proteasome inhibitor, to arrest the cells at metaphase (Fig. 2, Movie 2). In 32 of 34 control cells, the addition of CW069 did not affect spindle bipolarity, consistent with the result obtained for several other human cell lines (Watts et al., 2013). In contrast, 33 of 63 *ASPM* KO cells showed pole splitting within 3 h after drug treatment; multipolar spindles were formed, in which spindle MTs were stably associated with the split poles (Fig. 2A, arrowheads). We concluded that ASPM is necessary for pole organisation in the absence of full HSET activity.

Spindle poles were unfocused upon double depletion of ASPM and CDK5RAP2

The centrosome constitutes the focal point of spindle MTs at the pole in animal somatic cells. However, in flies and mammals, acentrosomal spindles with two focused poles can be assembled after centrosomal protein depletion/inhibition, indicating that centrosomes are not a prerequisite for pole focusing (Megraw et al., 2001; Wong et al., 2015). Nevertheless, centrosomes play a supportive role in spindle MT focusing, perhaps by supplying additional MTs for the motors and MAPs for the interaction (Baumbach et al., 2015; Chavali et al., 2016; Goshima et al., 2005; Heald et al., 1997; Ito and Goshima, 2015; Mountain et al., 1999; Silk et al., 2009; Wakefield et al., 2001). We hypothesised that lack of the pole unfocusing phenotype in the absence of ASPM may also be partly due to the presence of a sufficient amount of centrosomal MTs in this cell line.

To test this possibility, we aimed to deplete another microcephaly protein, CDK5RAP2 (also known as CEP215), which attaches the γ-tubulin ring complex (γ-TuRC) to the centrosome and activates γ-TuRC-dependent MT nucleation, in the *ASPM* KO line; CDK5RAP2 depletion reduces centrosomal MTs (Bond et al., 2005; Choi et al., 2010; Fong et al., 2008). To this end, we utilised the auxin-inducible degron (AID) system (Nishimura et al., 2009). We tagged endogenous CDK5RAP2 with mCherry and mini-AID (mAID) sequences in the HCT116 cells possessing the gene encoding *Oryza sativa* (Os) TIR1, the auxin responsive F-box protein that constitutes a functional SCF ubiquitin ligase in human cells (Fig. S2A–C). In this cell line, OsTIR1 protein was induced by doxycycline hyclate (Dox) (Natsume et al., 2016), and then CDK5RAP2-mAID-mCherry was degraded rapidly upon auxin (indole-3-acetic acid; IAA) addition to the culture medium (Fig. S2D). We observed spindle dynamics after 24 h of auxin treatment in the presence or absence of ASPM (Fig. 3A, Movie 3). We also analysed two control samples for this experiment. In the external control, the cells were not treated with Dox or IAA ('untreated' in Fig. 3B). In the internal control, CDK5RAP2 was not degraded in a subpopulation of the cells treated with Dox and IAA ('CDK5RAP2 remains' in Fig. 3B). In cells that had intact endogenous ASPM, bipolar spindles with focused poles were observed in 21 of 22 cases, and all went into anaphase with only a slight delay, even when CDK5RAP2-mAID-mCherry signals were hardly detected (Fig. 3A second row, 3B, NEBD to anaphase onset; 30 ± 8 min [±SD], n = 22). In the internal control samples with *ASPM* deleted, 22 of 23 cells had focused spindle poles and proceeded into anaphase without significant delay (Fig. 3A third row, 3B, 24 ± 3 min, n = 22). In sharp contrast, when CDK5RAP2-mAID-mCherry was depleted in the *ASPM* KO background, 66 of 83 cells exhibited unfocused spindle poles; spindle MTs were not persistently associated with the pole during metaphase (Fig. 3A bottom row, 3B). In these cells, anaphase onset was significantly delayed (NEBD to anaphase onset in 44 cells was >1 h). We concluded that ASPM is required for pole focusing

when the centrosome function is compromised.

A recent report showed that CDK5RAP2 binds to HSET and promotes association of HSET with the centrosome (Chavali et al., 2016). Therefore, the effect of CDK5RAP2 depletion may be partly attributed to reduction of the HSET activity at the centrosome. However, we interpret that other defects such as reduction of centrosomal MTs (Choi et al., 2010; Fong et al., 2008) also contribute to the synthetic effect with ASPM KO, since, unlike HSET-inhibited cells, MT focusing was not stably maintained at the pole during metaphase in CDK5RAP2-depleted cells (Fig. 3A bottom row).

RNAi depletion phenocopies CRISPR-based KO

One possible reason for the lack of mitotic defects in the *ASPM* KO line is that suppressor mutations were introduced into another locus during the few weeks of KO line selection. To exclude this possibility, we depleted ASPM more rapidly from the cell using RNAi. We prepared four independent siRNA constructs, one of which was previously reported to give rise to abnormal spindle orientation and mitotic progression in U2OS cells after 72 h (Higgins et al., 2010) (Table S1). Immunostaining using anti-ASPM antibody indicated that all constructs efficiently knocked down ASPM protein after 48 h in HCT116 cells; the intensity of the residual ASPM signal was similar among the four constructs and to that of the KO line (Fig. 4A, B). We observed a strong toxic effect for one of the constructs (siRNA #2) and mitotic acceleration for another (siRNA #3), suggesting that these constructs had off-target effects on important proteins other than ASPM (Table S1). However, cell proliferation, spindle morphogenesis, and mitotic progression were not defective for the remaining two constructs, reminiscent of the results observed in the KO line. These results strongly suggest that rapid ASPM depletion also has little impact on spindle organisation.

To test whether the synthetic phenotype with CDK5RAP2 depletion is also observed for *ASPM* RNAi, we treated the cells with three *ASPM* siRNAs (excluding the toxic siRNA construct) and then degraded CDK5RAP2 with the AID system. Time-lapse imaging indicated that pole unfocusing was frequently caused by CDK5RAP2 degradation for each siRNA construct (Fig. 4C). These results support the conclusion that ASPM becomes critical only when the centrosome function is compromised.

Microcephaly mutation in *ASPM* causes pole unfocusing in the absence of CDK5RAP2

Homozygous mutations in the *ASPM* gene have been identified at various positions in microcephaly patients, almost all of which introduce a premature stop codon in the gene (Abdel-Hamid et al., 2016; Bond et al., 2002; Bond et al., 2003; Nicholas et al., 2009; Tan et al., 2014). The two most C-terminal mutations identified in three previous studies were located in front of the HEAT repeat motif: a nonsense mutation at amino acid (aa) 3,233 and a 1-bp deletion at aa 3,252, which introduces a stop codon at aa 3,261 (Fig. 5A). To test the effect of microcephaly mutations in spindle pole organisation, we inserted mClover next to the aa 3,232 residue to closely mimic a patient mutation (Fig. 5A, Fig. S3A, C); we selected this mutation, and not the most C-terminal mutation, as the former site was located next to the CRISPR-friendly sequences. As the control, mClover was inserted at the C-terminus of the *ASPM* gene (Fig. S3B). As expected, several replacement lines were obtained for both constructs. ASPM [1–3,232]-mClover showed indistinguishable localisation at the pole from that of the full-length ASPM-mClover, consistent with the case of *Drosophila* Asp where the HEAT repeat was shown to be unnecessary for MT minus-end localisation (Ito and Goshima, 2015). However, when CDK5RAP2 was depleted by the AID system, we observed a severe pole unfocusing phenotype for the ASPM [1–3,232]-mClover line, reminiscent of the results for the *ASPM* KO line (Fig. 5B, C; Movie 4). Thus, the mutation that mimics that of microcephaly patients impaired the function of ASPM in pole organisation. Since other mutations in patients were identified upstream of the introduced mutation, a similar pole-unfocusing phenotype is expected to be observed for all cases.

Discussion

The results described above established that human ASPM, like the *Drosophila* orthologue Asp, is a spindle pole-focusing factor. ASPM/Asp would localise to and cross-link adjacent MT minus ends. However, unlike Asp in *Drosophila*, the depletion of which gives rise to severe phenotypes in various cell types and causes brain size reduction as well as lethality (Ripoll et al., 1985; Rujano et al., 2013; Saunders et al., 1997; Schoborg et al., 2015; Wakefield et al., 2001), ASPM was not essential in the human HCT116 cell line (derived from a patient with colorectal carcinoma). Our data indicated that ASPM becomes indispensable for pole organisation when the activity of kinesin-14 or a centrosomal MT nucleation factor is suppressed; normally, kinesin-14 and CDK5RAP2 are active enough to mask the function of ASPM in this cell type. This scenario may hold true for many other cell types in mammals. In a mouse model, mutations in *Aspm* cause a reduction in brain and testis/ovary sizes but do not cause lethality (Fujimori et al., 2014; Pulvers et al., 2010). In general, mutations in critical spindle assembly factors lead to severe developmental problem, which are often associated with early embryonic lethality, as mitosis is a crucial event throughout animal development (Aguirre-Portoles et al., 2012; Castillo and Justice, 2007; Silk et al.,

2009; Watanabe et al., 2016). The lack of embryonic lethality caused by mutations in *ASPM* and other pole-organising factors linked to microcephaly (e.g. CDK5RAP2, SAS-4) may be attributed to the highly redundant nature of pole organisation in mammals. Supporting this idea, a cell type-specific polar defect has been observed for another pole-focusing factor, NuMA (Seldin et al., 2016; Silk et al., 2009). Thus, it is tempting to speculate that certain neuronal cell types in humans more heavily rely on ASPM for pole organisation than on other factors, and therefore a severe phenotype only appears in the brain of the patients.

A model for the cause of microcephaly postulates a defect in spindle orientation and asymmetric cell division (Feng and Walsh, 2004; Fish et al., 2008; Fish et al., 2006; Gai et al., 2016; Lizarraga et al., 2010; Thornton and Woods, 2009). Consistent with this idea, spindle orientation error was reported following *ASPM* RNAi in human U2OS cells (Higgins et al., 2010). However, depletion of other proteins required for spindle orientation (LGN, aPKCλ) does not cause microcephaly in the mouse model (Imai et al., 2006; Konno et al., 2008; Megraw et al., 2011). Moreover, a recent study using a *Sas-4* mutant mouse model suggested that microcephaly is caused by mitotic delay and apoptosis, independent of spindle orientation (Insolera et al., 2014). The results of the present study raise the possibility that spindle pole disorganisation is a cause of the severe mitotic delay that leads to microcephaly.

Materials and Methods

Plasmid construction Plasmid information is described in Table S4. pX330-U6-Chimeric_BB-CBh-hSpCas9 (Addgene #42230 (Cong et al., 2013)) was used to construct CRISPR/Cas9 vectors according to the protocol of (Ran et al., 2013). PAM and 20-bp sgRNA sequences were selected by the Optimized CRISPR Design tool (http://crispr.mit.edu) (Table S2).

Cell culture and line selection The original HCT116 cell line and the HCT116 cells expressing OsTIR1 under the conditional Tet promoter and the puromycin-resistant gene (HCT116 Tet-OsTIR1) were cultured in McCoy's 5A medium (Gibco) supplemented with 10% foetal bovine serum (Gibco) and 1% penicillin-streptomycin-amphotericin B suspension (Wako) (cells were obtained from Dr M. Kanemaki) (Natsume et al., 2016). Cells were maintained in a 37°C humid incubator with 5% CO_2. Effectine (Qiagen) was used for plasmid transfection. For the construction of the *ASPM* KO line, a CRISPR/Cas9 plasmid (pAI112) with sgRNA and SpCas9 sequences, and a donor plasmid (pAI114) harbouring the neomycin-resistant gene flanked by homologous sequences were transfected into the original HCT116 cell line. The complete *ASPM* KO line (KO^C) was selected by co-transfection of the following two plasmids into the original HCT116 cell: a CRISPR/Cas9 plasmid (pAI119) that contains two sets of sgRNA and SpCas9 targeting the N- and C-terminal regions, and a donor plasmid (pAI118) that has the neomycin-resistant gene flanked by homologous sequences. mAID-tagged cell lines expressing CDK5RAP2-mAID-mCherry were generated according to the procedures described in (Natsume et al., 2016). In brief, the HCT116 Tet-OsTIR1 line was transfected with a CRISPR/Cas9 plasmid (pTK478) and a donor plasmid (pTK472) carrying mAID-mCherry and a hygromycin-resistant gene flanked by homologous sequences. The ASPM-KO/CDK5RAP2-mAI-mCherry line was selected by co-transfection of the CRISPR/Cas9 plasmid (pAI112) and the donor plasmid (pAI114) into the CDK5RAP2-mAID-mCherry expression line. ASPM-mClover and ASPM [1-3232]-mClover lines were selected by co-transfection of the CRISPR/Cas9 plasmid (pAI113, pAI121) and the donor plasmid (pAI110, pAI120) harbouring mClover and neomycin-resistant genes flanked by homologous sequences into the CDK5RAP2-mAID-mCherry expression line. Two to three days after transfection, the cells were plated on 10-cm culture dishes and cultured in selection medium containing 200 μg/ml hygromycin (Wako), 1 μg/ml puromycin (Wako), and/or 800 μg/ml G-418 (Roche) for 10–18 days. Single colonies were picked up for further selection in a 24-well plate. To confirm homozygous insertion, genomic DNAs were prepared from drug-resistant clones for most lines, whereas the cells were directly used as PCR templates for checking the ASPM-mClover lines (full-length and C-terminal truncation). PCR was performed using Tks Gflex DNA polymerase (TaKaRa) and corresponding primers (Table S3), as described by (Natsume et al., 2016). Proper tagging of mClover to *ASPM* was also verified by DNA sequencing after PCR.

AID To degrade mAID-tagged CDK5RAP2, the cells were treated with 2 μg/ml Dox (Sigma) for 24 h to induce the expression of OsTIR1, and with 500 μM IAA (Wako) for 24 h to induce the degradation of CDK5RAP2-mAID-mCherry (Natsume et al., 2016).

RNAi siRNA transfection was carried out using Lipofectamine RNAiMAX (Invitrogen). In the ASPM depletion experiment, HCT116 cells were incubated with 13.3 nM *ASPM* or control luciferase siRNA for 42 h (live imaging) or 48 h (immunostaining). The primers for siRNA constructs are shown in Table S1 (note that we observed a possible off-target effect for at least two of the constructs). For live imaging after mAID-tagged CDK5RAP2 degradation, Dox and IAA were added to the culture at 24 h after siRNA transfection.

Microscopy, image analysis, and data presentation Live imaging was performed using spinning-disc confocal microscopy with a 60× 1.40 NA objective lens. A CSU-X1 confocal unit (Yokogawa, Japan) attached to a Nikon Ti inverted microscope, EMCCD camera ImagEM (Hamamatsu, Japan) that was cooled (–80°C) with a chiller (Julabo USA Inc.), and a stage chamber were used for image acquisition (37°C, 5% CO_2). Characterisation of the phenotypes of fixed samples was performed with the Nikon Ti inverted microscope attached to the EMCCD camera Evolve (Roper). Three objective lenses (100× 1.49 NA, 100× lens 1.45 NA, or 40× 1.30 NA) were used. The microscopes and attached devices were controlled using Micromanager. Images were analysed with ImageJ.

For live imaging, the MTs were stained with SiR-Tubulin (30 nM; Spirochrome) for >1 h prior to image acquisition. For HSET inhibition, MG132 (10 μM; Wako) was first added to the culture medium together with SiR-Tubulin at >1 h prior to imaging, and then CW069 (200 μM; Selleck Chemicals) was supplied. Immunostaining was performed according to the standard procedure using 6.4% paraformaldehyde, and anti-tubulin (YOL1/34, 1:500, rat monoclonal, AbD Serotec) and anti-ASPM (1:1,000, rabbit polyclonal, antigen [aa 3,425–3,477], Bethyl Laboratories, Inc.) antibodies. DNA was stained with DAPI. The fluorescence intensity of polar ASPM was measured from a single-plane image of the immunostained samples, with measurements taken from the cell's most in-focus pole. Background intensity was subtracted from each measurement. Multiple images presented in a comparative manner in figures and movies were acquired and processed in an identical manner, except for those in Fig. 4A, in which SiR-tubulin staining in the ASPM #2 sample was stronger than the others, perhaps due to massive cell death induced by this specific siRNA; thus, the images were acquired with a shorter laser exposure for this particular sample. Graphical presentation of the data and statistical analysis were performed with the GraphPad Prism 6.0 software.

Immunoblotting Protein extracts were prepared according to a previously described protocol (Ito and Goshima, 2015). In brief, the cells were treated with the Cytobuster (EMD Millipore) solution, which also contained benzonase, dithiothreitol, and protease inhibitors (30 min on ice), followed by addition of the urea-containing solution (62.5 mM Tris, pH 6.8, 10% glycerol, 2% SDS, 4 M urea, and 2-mercaptoethanol) at room temperature (5 h). Immunoblotting was carried out with anti-CDK5RAP2 (1:10,000, rabbit polyclonal, Abcam).

Acknowledgements

We are grateful to Toyoaki Natsume and Masato Kanemaki (National Institute of Genetics, Japan) for reagents and technical advice, and to Momoko Nishina (Nagoya University, Japan) for technical assistance. This work was supported by the Uehara Memorial Foundation and Takeda Science Foundation (to G.G.). A.I. is a recipient of a JSPS pre-doctoral fellowship. The authors declare no competing financial interests.

Supplementary Movie legends

Movie 1. Normal spindle formation and mitotic progression after *ASPM* KO
SiR-tubulin images were acquired every 3 min with spinning-disc confocal microscopy. Images were acquired with 5 z-sections (separated by 3 μm) and displayed after maximum projection. Time 0 corresponds to the timing of nuclear envelope breakdown. The images of two 'incomplete' KO lines (#4 and #23) and two 'complete' KO lines (#25 and #27) are presented.

Movie 2. HSET inhibition induced spindle pole splitting in the absence of ASPM
SiR-tubulin images were acquired every 3 min with spinning-disc confocal microscopy. Images were acquired with 5 z-sections (separated by 3 μm) and displayed after maximum projection. Time 0 corresponds to the timing of CW069 (HSET inhibitor) addition. Two ASPM KO lines (#4 and #23) were used.

Movie 3. CDK5RAP2 degradation impairs spindle pole focusing and mitotic progression in the absence of ASPM
Images were acquired every 3 min with spinning-disc confocal microscopy. Green, CDK5RAP2-mAID-mCherry; magenta, Sir-Tubulin. Images were acquired with 5 z-sections (separated by 3 μm) and displayed after maximum projection. Time 0 corresponds to the timing of nuclear envelope breakdown.

Movie 4. Microcephaly mutation of ASPM impairs spindle focusing and mitotic progression in the absence of CDK5RAP2
Images were acquired every 5 min with spinning-disc confocal microscopy. Yellow, CDK5RAP2-mAID-mCherry; magenta, Sir-Tubulin; cyan, ASPM-mClover (full-length or C-terminal truncation that mimics microcephaly mutations). Images were acquired with 5 z-sections (separated by 3 μm) and displayed after maximum projection. Time 0 corresponds to the timing of nuclear envelope breakdown.

References

Abdel-Hamid, M.S., M.F. Ismail, H.A. Darwish, L.K. Effat, M.S. Zaki, and G.M. Abdel-Salam. 2016. Molecular and phenotypic spectrum of ASPM-related primary microcephaly: Identification of eight novel mutations. *Am J Med Genet A*. 170:2133-2140.

Aguirre-Portoles, C., A.W. Bird, A. Hyman, M. Canamero, I. Perez de Castro, and M. Malumbres. 2012. Tpx2 controls spindle integrity, genome stability, and tumor development. *Cancer Res*. 72:1518-1528.

Baumbach, J., Z.A. Novak, J.W. Raff, and A. Wainman. 2015. Dissecting the function and assembly of acentriolar microtubule organizing centers in Drosophila cells in vivo. *PLoS Genet*. 11:e1005261.

Bond, J., E. Roberts, G.H. Mochida, D.J. Hampshire, S. Scott, J.M. Askham, K. Springell, M. Mahadevan, Y.J. Crow, A.F. Markham, C.A. Walsh, and C.G. Woods. 2002. ASPM is a major determinant of cerebral cortical size. *Nat Genet*. 32:316-320.

Bond, J., E. Roberts, K. Springell, S.B. Lizarraga, S. Scott, J. Higgins, D.J. Hampshire, E.E. Morrison, G.F. Leal, E.O. Silva, S.M. Costa, D. Baralle, M. Raponi, G. Karbani, Y. Rashid, H. Jafri, C.

Bennett, P. Corry, C.A. Walsh, and C.G. Woods. 2005. A centrosomal mechanism involving CDK5RAP2 and CENPJ controls brain size. *Nat Genet*. 37:353-355.

Bond, J., S. Scott, D.J. Hampshire, K. Springell, P. Corry, M.J. Abramowicz, G.H. Mochida, R.C. Hennekam, E.R. Maher, J.P. Fryns, A. Alswaid, H. Jafri, Y. Rashid, A. Mubaidin, C.A. Walsh, E. Roberts, and C.G. Woods. 2003. Protein-truncating mutations in ASPM cause variable reduction in brain size. *Am J Hum Genet*. 73:1170-1177.

Castillo, A., and M.J. Justice. 2007. The kinesin related motor protein, Eg5, is essential for maintenance of pre-implantation embryogenesis. *Biochem Biophys Res Commun*. 357:694-699.

Chavali, P.L., G. Chandrasekaran, A.R. Barr, P. Tatrai, C. Taylor, E.K. Papachristou, C.G. Woods, S. Chavali, and F. Gergely. 2016. A CEP215-HSET complex links centrosomes with spindle poles and drives centrosome clustering in cancer. *Nat Commun*. 7:11005.

Choi, Y.K., P. Liu, S.K. Sze, C. Dai, and R.Z. Qi. 2010. CDK5RAP2 stimulates microtubule nucleation by the gamma-tubulin ring complex. *J Cell Biol*. 191:1089-1095.

Cong, L., F.A. Ran, D. Cox, S. Lin, R. Barretto, N. Habib, P.D. Hsu, X. Wu, W. Jiang, L.A. Marraffini, and F. Zhang. 2013. Multiplex genome engineering using CRISPR/Cas systems. *Science*. 339:819-823.

Feng, Y., and C.A. Walsh. 2004. Mitotic spindle regulation by Nde1 controls cerebral cortical size. *Neuron*. 44:279-293.

Fish, J.L., C. Dehay, H. Kennedy, and W.B. Huttner. 2008. Making bigger brains-the evolution of neural-progenitor-cell division. *J Cell Sci*. 121:2783-2793.

Fish, J.L., Y. Kosodo, W. Enard, S. Paabo, and W.B. Huttner. 2006. Aspm specifically maintains symmetric proliferative divisions of neuroepithelial cells. *Proc Natl Acad Sci U S A*. 103:10438-10443.

Fong, K.W., Y.K. Choi, J.B. Rattner, and R.Z. Qi. 2008. CDK5RAP2 is a pericentriolar protein that functions in centrosomal attachment of the gamma-tubulin ring complex. *Mol Biol Cell*. 19:115-125.

Fujimori, A., K. Itoh, S. Goto, H. Hirakawa, B. Wang, T. Kokubo, S. Kito, S. Tsukamoto, and S. Fushiki. 2014. Disruption of Aspm causes microcephaly with abnormal neuronal differentiation. *Brain Dev*. 36:661-669.

Gaglio, T., A. Saredi, J.B. Bingham, M.J. Hasbani, S.R. Gill, T.A. Schroer, and D.A. Compton. 1996. Opposing motor activities are required for the organization of the mammalian mitotic spindle pole. *J Cell Biol*. 135:399-414.

Gai, M., F.T. Bianchi, C. Vagnoni, F. Verni, S. Bonaccorsi, S. Pasquero, G.E. Berto, F. Sgro, A.M. Chiotto, L. Annaratone, A. Sapino, A. Bergo, N. Landsberger, J. Bond, W.B. Huttner, and F. Di Cunto. 2016. ASPM and CITK regulate spindle orientation by affecting the dynamics of astral microtubules. *EMBO Rep*. 17:1396-1409.

Goshima, G., F. Nedelec, and R.D. Vale. 2005. Mechanisms for focusing mitotic spindle poles by minus end-directed motor proteins. *J Cell Biol*. 171:229-240.

Hatsumi, M., and S.A. Endow. 1992. Mutants of the microtubule motor protein, nonclaret disjunctional, affect spindle structure and chromosome movement in meiosis and mitosis. *J Cell Sci*. 101 (Pt 3):547-559.

Heald, R., R. Tournebize, A. Habermann, E. Karsenti, and A. Hyman. 1997. Spindle assembly in Xenopus egg extracts: respective roles of centrosomes and microtubule self-organization. *J Cell Biol*. 138:615-628.

Higgins, J., C. Midgley, A.M. Bergh, S.M. Bell, J.M. Askham, E. Roberts, R.K. Binns, S.M. Sharif, C. Bennett, D.M. Glover, C.G. Woods, E.E. Morrison, and J. Bond. 2010. Human ASPM participates in spindle organisation, spindle orientation and cytokinesis. *BMC Cell Biol*. 11:85.

Imai, F., S. Hirai, K. Akimoto, H. Koyama, T. Miyata, M. Ogawa, S. Noguchi, T. Sasaoka, T. Noda, and S. Ohno. 2006. Inactivation of aPKClambda results in the loss of adherens junctions in neuroepithelial cells without affecting neurogenesis in mouse neocortex. *Development*. 133:1735-1744.

Insolera, R., H. Bazzi, W. Shao, K.V. Anderson, and S.H. Shi. 2014. Cortical neurogenesis in the absence of centrioles. *Nat Neurosci*. 17:1528-1535.

Ito, A., and G. Goshima. 2015. Microcephaly protein Asp focuses the minus ends of spindle microtubules at the pole and within the spindle. *J Cell Biol*. 211:999-1009.

Konno, D., G. Shioi, A. Shitamukai, A. Mori, H. Kiyonari, T. Miyata, and F. Matsuzaki. 2008. Neuroepithelial progenitors undergo LGN-dependent planar divisions to maintain self-renewability during mammalian neurogenesis. *Nat Cell Biol*. 10:93-101.

Kouprina, N., A. Pavlicek, N.K. Collins, M. Nakano, V.N. Noskov, J. Ohzeki, G.H. Mochida, J.I. Risinger, P. Goldsmith, M. Gunsior, G. Solomon, W. Gersch, J.H. Kim, J.C. Barrett, C.A. Walsh, J. Jurka, H. Masumoto, and V. Larionov. 2005. The microcephaly ASPM gene is expressed in proliferating tissues and encodes for a mitotic spindle protein. *Hum Mol Genet*. 14:2155-2165.

Lizarraga, S.B., S.P. Margossian, M.H. Harris, D.R. Campagna, A.P. Han, S. Blevins, R. Mudbhary, J.E. Barker, C.A. Walsh, and M.D. Fleming. 2010. Cdk5rap2 regulates centrosome function and chromosome segregation in neuronal progenitors. *Development*. 137:1907-1917.

Manning, A.L., and D.A. Compton. 2007. Mechanisms of spindle-pole organization are influenced by kinetochore activity in mammalian cells. *Curr Biol*. 17:260-265.

Megraw, T.L., L.R. Kao, and T.C. Kaufman. 2001. Zygotic development without functional mitotic centrosomes. *Curr Biol*. 11:116-120.

Megraw, T.L., J.T. Sharkey, and R.S. Nowakowski. 2011. Cdk5rap2 exposes the centrosomal root of microcephaly syndromes. *Trends Cell Biol*. 21:470-480.

Merdes, A., R. Heald, K. Samejima, W.C. Earnshaw, and D.W. Cleveland. 2000. Formation of spindle poles by dynein/dynactin-dependent transport of NuMA. *J Cell Biol*. 149:851-862.

Morales-Mulia, S., and J.M. Scholey. 2005. Spindle pole organization in Drosophila S2 cells by dynein, abnormal spindle protein (Asp), and KLP10A. *Mol Biol Cell*. 16:3176-3186.

Mountain, V., C. Simerly, L. Howard, A. Ando, G. Schatten, and D.A. Compton. 1999. The kinesin-related protein, HSET, opposes the activity of Eg5 and cross-links microtubules in the mammalian mitotic spindle. *J Cell Biol*. 147:351-366.

Natsume, T., T. Kiyomitsu, Y. Saga, and M.T. Kanemaki. 2016. Rapid Protein Depletion in Human Cells by Auxin-Inducible Degron Tagging with Short Homology Donors. *Cell Rep*. 15:210-218.

Nicholas, A.K., E.A. Swanson, J.J. Cox, G. Karbani, S. Malik, K. Springell, D. Hampshire, M. Ahmed, J. Bond, D. Di Benedetto, M. Fichera, C. Romano, W.B. Dobyns, and C.G. Woods. 2009. The molecular landscape of ASPM mutations in primary microcephaly. *J Med Genet*. 46:249-253.

Nishimura, K., T. Fukagawa, H. Takisawa, T. Kakimoto, and M. Kanemaki. 2009. An auxin-based degron system for the rapid depletion of proteins in nonplant cells. *Nat Methods*. 6:917-922.

Paramasivam, M., Y.J. Chang, and J.J. LoTurco. 2007. ASPM and citron kinase co-localize to the midbody ring during cytokinesis. *Cell Cycle*. 6:1605-1612.

Pulvers, J.N., J. Bryk, J.L. Fish, M. Wilsch-Brauninger, Y. Arai, D. Schreier, R. Naumann, J. Helppi, B. Habermann, J. Vogt, R. Nitsch, A. Toth, W. Enard, S. Paabo, and W.B. Huttner. 2010. Mutations in mouse Aspm (abnormal spindle-like microcephaly associated) cause not only microcephaly but also major defects in the germline. *Proc Natl Acad Sci U S A*. 107:16595-16600.

Ran, F.A., P.D. Hsu, J. Wright, V. Agarwala, D.A. Scott, and F. Zhang. 2013. Genome engineering using the CRISPR-Cas9 system. *Nat Protoc*. 8:2281-2308.

Ripoll, P., S. Pimpinelli, M.M. Valdivia, and J. Avila. 1985. A cell division mutant of Drosophila with a functionally abnormal spindle. *Cell*. 41:907-912.

Rujano, M.A., L. Sanchez-Pulido, C. Pennetier, G. le Dez, and R. Basto. 2013. The microcephaly protein Asp regulates neuroepithelium morphogenesis by controlling the spatial distribution of myosin II. *Nat Cell Biol*. 15:1294-1306.

Saunders, R.D., M.C. Avides, T. Howard, C. Gonzalez, and D.M. Glover. 1997. The Drosophila gene abnormal spindle encodes a novel microtubule-associated protein that associates with the polar regions of the mitotic spindle. *J Cell Biol*. 137:881-890.

Schoborg, T., A.L. Zajac, C.J. Fagerstrom, R.X. Guillen, and N.M. Rusan. 2015. An Asp-CaM complex is required for centrosome-pole cohesion and centrosome inheritance in neural stem cells. *J Cell Biol*. 211:987-998.

Seldin, L., A. Muroyama, and T. Lechler. 2016. NuMA-microtubule interactions are critical for spindle orientation and the morphogenesis of diverse epidermal structures. *Elife*. 5.

Silk, A.D., A.J. Holland, and D.W. Cleveland. 2009. Requirements for NuMA in maintenance and establishment of mammalian spindle poles. *J Cell Biol*. 184:677-690.

Tan, C.A., D. del Gaudio, M.A. Dempsey, K. Arndt, S. Botes, A. Reeder, and S. Das. 2014. Analysis of ASPM in an ethnically diverse cohort of 400 patient samples: perspectives of the molecular diagnostic laboratory. *Clin Genet*. 85:353-358.

Thornton, G.K., and C.G. Woods. 2009. Primary microcephaly: do all roads lead to Rome? *Trends Genet*. 25:501-510.

Wakefield, J.G., S. Bonaccorsi, and M. Gatti. 2001. The drosophila protein asp is involved in microtubule organization during spindle formation and cytokinesis. *J Cell Biol*. 153:637-648.

Walczak, C.E., I. Vernos, T.J. Mitchison, E. Karsenti, and R. Heald. 1998. A model for the proposed roles of different microtubule-based motor proteins in establishing spindle bipolarity. *Curr Biol*. 8:903-913.

Watanabe, S., G. Shioi, Y. Furuta, and G. Goshima. 2016. Intra-spindle Microtubule Assembly Regulates Clustering of Microtubule-Organizing Centers during Early Mouse Development. *Cell Rep*. 15:54-60.

Watts, C.A., F.M. Richards, A. Bender, P.J. Bond, O. Korb, O. Kern, M. Riddick, P. Owen, R.M. Myers, J. Raff, F. Gergely, D.I. Jodrell, and S.V. Ley. 2013. Design, synthesis, and biological evaluation of an allosteric inhibitor of HSET that targets cancer cells with supernumerary centrosomes. *Chem Biol*. 20:1399-1410.

Wong, Y.L., J.V. Anzola, R.L. Davis, M. Yoon, A. Motamedi, A. Kroll, C.P. Seo, J.E. Hsia, S.K. Kim, J.W. Mitchell, B.J. Mitchell, A. Desai, T.C. Gahman, A.K. Shiau, and K. Oegema. 2015. Cell biology. Reversible centriole depletion with an

inhibitor of Polo-like kinase 4. *Science*. 348:1155-1160.

Zhong, X., L. Liu, A. Zhao, G.P. Pfeifer, and X. Xu. 2005. The abnormal spindle-like, microcephaly-associated (ASPM) gene encodes a centrosomal protein. *Cell Cycle*. 4:1227-1229.

Table S1. Primers for RNAi

siRNA	Sequences	Note
ASPM -1	UGCCAUGGUGCAACUUGCU	(Higgins et al., 2010)
ASPM -2	GCACAUUAUGAAGGUCAAACUGGACUGUGC	HSS138109 (Invitrogen) Toxic effect
ASPM -3	GCGCUUUUAGGCUGCAACACGAAACAGCGC	HSS138110 (Invitrogen) Shorter mitosis
ASPM -4	GGAGAAAUUCUUGCAGCUUUCUCUCUCUCC	HSS138111 (Invitrogen)

Table S2. sgRNA sequences for CRISPR/Cas9-mediated genome editing

Gene	sgRNA	PAM
ASPM (N-terminus)	TGCCATGGCGAACCGGCGAG	TGG
ASPM (C-terminus)	CAAATGGTGATGGATACGCT	TGG
ASPM (mutation insertion)	CATTATGGAGAGGCTATTCT	TGG
CDK5RAP2 (C-terminus)	AAGAGACAGCGTGAGCTCGG	TGG

Table S3. PCR primers to confirm gene editing

Gene	Primer sequences (5'-3')	
ASPM (N-terminus)	TTGCGAGTTTATTGGGCTTG	Fig. 1A,S1B
	AGGGTTGTCTAGGGCCAG	Fig. 1A,S1B
ASPM (C-terminus)	TCTCCCACCTCTTTGAGC	Fig. S1B,S3B
	AATCATCTTATGACATATTAGTTTATTACATGC	Fig. S1B,S3B
ASPM (mutation insert)	TGGTCGATAAATGCTGTCC	Fig. S3A
	AGAAATTGCTCCACTCTGG	Fig. S3A
CDK5RAP2 (C-terminus)	GGTAAATATTTACTGACCAAAC	Fig. S2A
	GGTGCCTGCCCCTGATC	Fig. S2A
Neomycin	CCTAGGCTTTTGCAAAGATCGATC	Fig. S1B

Table S4. Plasmids constructed and used in this study

lines	gRNA plasmid	Donor vector
ASPM-KO	pAI112	pAI114
ASPM-KO^{C}	pAI119	pAI118
ASPM-mClover	pAI113	pAI110
ASPM[1-3232]-mClover	pAI121	pAI120
CDK5RAP2-mAID-mCherry	pTK478	pTK472

Plasmid	Vector information	Description
pAI110	pAI109, which contained each ~800-bp DNA sequence of the *ASPM* gene flanking the stop codon in exon 28. The vector of this plasmid was pCR2.1-TOPO. The sequences corresponding to sgRNA and PAM were altered to encode amino	The BamHI fragment containing mClover and the neomycin-resistant gene were extracted from pMK277 (a gift from Dr M. Kanemaki (Natsume et al., 2016)), and inserted into the BamHI site of pAI109.

	acids, and a BamHI site was inserted in front of the stop codon.	
pAI112	pX330	The following two oligos containing 20-nt guide sequence were annealed and inserted into the BbsI site of pX330: CACCGtgccatggcgaaccggcgag (top) and AAACctcgccggttcgccatggcaC (bottom)
pAI113	pX330	The following two oligos containing 20-nt guide sequence were annealed and inserted into the BbsI site of pX330: CACCGcaaatggtgatggatacgct (top) and AAACagcgtatccatcaccatttgC (bottom)
pAI114	pAI108, the donor vector of mClover-ASPM that contained mClover, the blasticidin-resistant gene, and each ~850-bp DNA sequence of the *ASPM* gene flanking the start codon in exon 1. The vector of this plasmid was pCR2.1-TOPO.	The ~850-bp DNA sequences after the start codon of the *ASPM* gene were amplified by genomic PCR, in which AscI and XhoI sites were added. The neomycin-resistant gene that contained AscI/NotI sites was purified from pAI110. These two fragments were inserted into the NotI/XhoI sites of pAI108, which contained the upstream sequences of the *ASPM* gene. The sequences corresponding to sgRNA, PAM, and the start codon were deleted (see Fig. 1A).
pAI118	pAI114	The ~800-bp DNA sequences of the *ASPM* gene that contained AscI/XhoI sites and the *ASPM* 3' untranslated region (UTR) of exon 28 were obtained from pAI110 and inserted into the AscI/XhoI sites of pAI114, which contained the *ASPM* 5' UTR of exon 1 and the neomycin-resistant gene. Note that the sequences of sgRNAs, PAMs, and start/stop codons were not included in this plasmid (see Fig. S1B).
pAI119	pAI112	The XbaI fragment containing the U6 promoter, 20-nt guide sequence targeting the C-terminal region of ASPM, and gRNA scaffold were purified from pAI113 and inserted into the XbaI site of pAI112.
pAI120	pCR2.1-TOPO	Four fragments were connected with In-Fusion HD Cloning Kit (Clontech® Laboratories, Inc). (1, 2) Each ~750-bp DNA sequence of the *ASPM* gene flanking the mutation site in exon 24 (see Fig. S3A) was amplified by genomic PCR (note that the sequences of sgRNA, PAM, and the region between sgRNA and the mutation site were altered to encode amino acids). (3) The BamHI fragment containing mClover and the neomycin-resistant gene was purified from pAI110. (4) The KpnI/XhoI fragment was extracted from pCR2.1-TOPO.
pAI121	pX330	The following two oligo DNAs containing 20-nt guide sequence were annealed and inserted into the BbsI site of pX330: CACCGcattatggagaggctattct (top) and AAACagaatagcctctccataatgC (bottom)
pTK472	pUC57-amp, ~400-bp DNA sequences containing the last exon of the *CDK5RAP2* gene (190,738–191,188: NC_000009) were synthesised. The STOP codon (tga) was mutated and replaced by (Gga GGA TCC) to insert a BamHI site. The sequences corresponding to sgRNA and PAM were deleted.	The BamHI fragment containing mAID-mCherry and the hygomycin-resistant gene was purified from pMK293 (a gift from Dr M. Kanemaki (Natsume et al., 2016)) and inserted into the BamHI site of the synthesised vector plasmid.
pTK478	pX330	The following two oligos containing 20-nt guide sequence were annealed and inserted into the BbsI site of pX330: CACCGaagagacagcgtgagctcgg (top) and AAACccgagctcacgctgtctcttC (bottom)

Figure 1

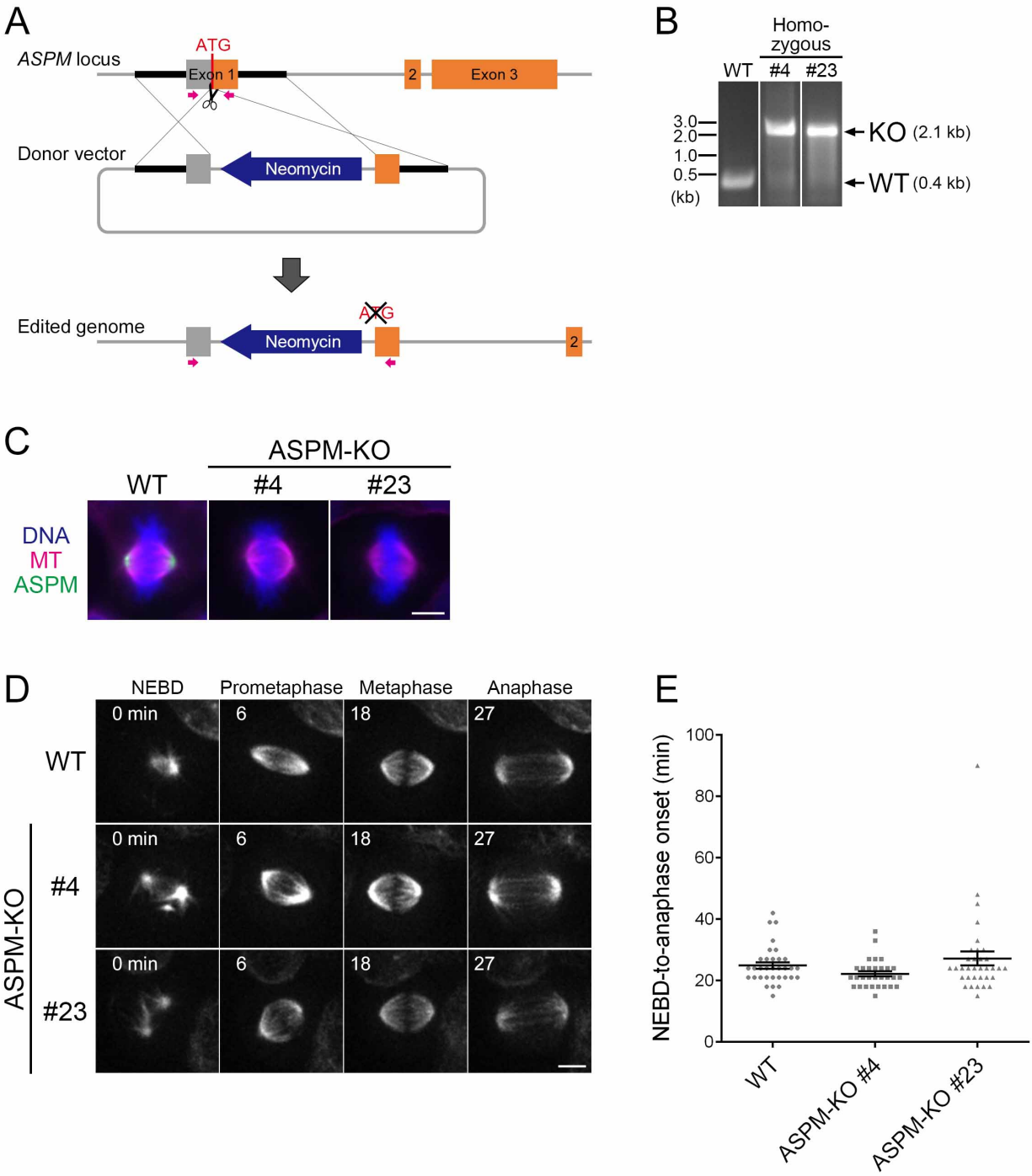

Figure 1. The ASPM KO line shows no mitotic defects
(A, B) Construction of the *ASPM* KO line, in which the region surrounding the start codon at the first exon of the *ASPM* gene was replaced by the neomycin-resistant marker. Targeted integration of the marker cassette was confirmed by PCR (primers are indicated as magenta arrows). **(C)** Immunofluorescence microscopy confirmed the diminishment of the ASPM signal at the spindle pole in two selected KO lines (clones #4 and #23). **(D)** Spindle dynamics of *ASPM* KO lines. MTs were visualized by SiR-tubulin staining. Images were acquired with 5 z-sections (separated by 3 μm) and displayed after maximum projection. No abnormality was detected. See also Movie 1. (E) Mitotic duration with or without ASPM. Data represent the mean ± SEM. WT; 25 ± 1 (n = 33), KO #4; 22 ± 1 (n = 30, $p > 0.05$, Student's t-test), KO #23; 27 ± 2 (n = 34, $p > 0.3$). Bars, 5 μm.

Figure 2

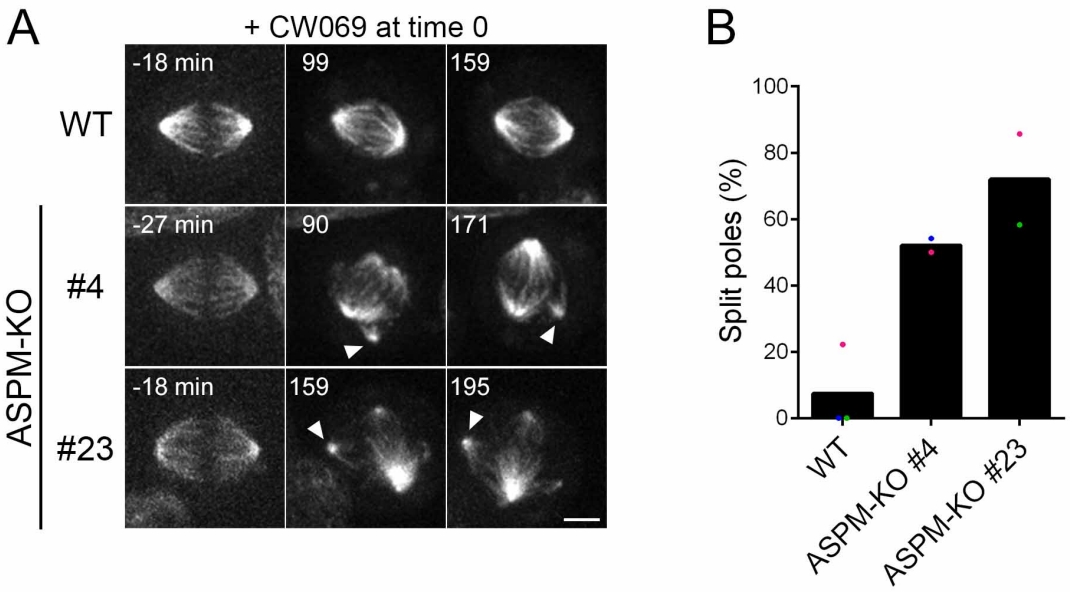

Figure 2. Spindle pole splitting upon double inhibition of ASPM and HSET
(A) Spindle morphology before and after addition of the HSET inhibitor (CW069, 200 µM). MTs were visualized by SiR-tubulin staining. Arrowheads indicate split poles. Images were acquired with 5 z-sections (separated by 3 µm) and displayed after maximum projection. Two independent KO lines were analysed (clones #4 and #23). See also Movie 2. Bar, 5 µm. **(B)** Frequency of split poles after CW069 addition. The values of each experiment are indicated by coloured dots, whereas the mean values of 2–3 independent experiments are indicated by black bars. Overall, 7–24 spindles were analysed in each experiment.

Figure 3

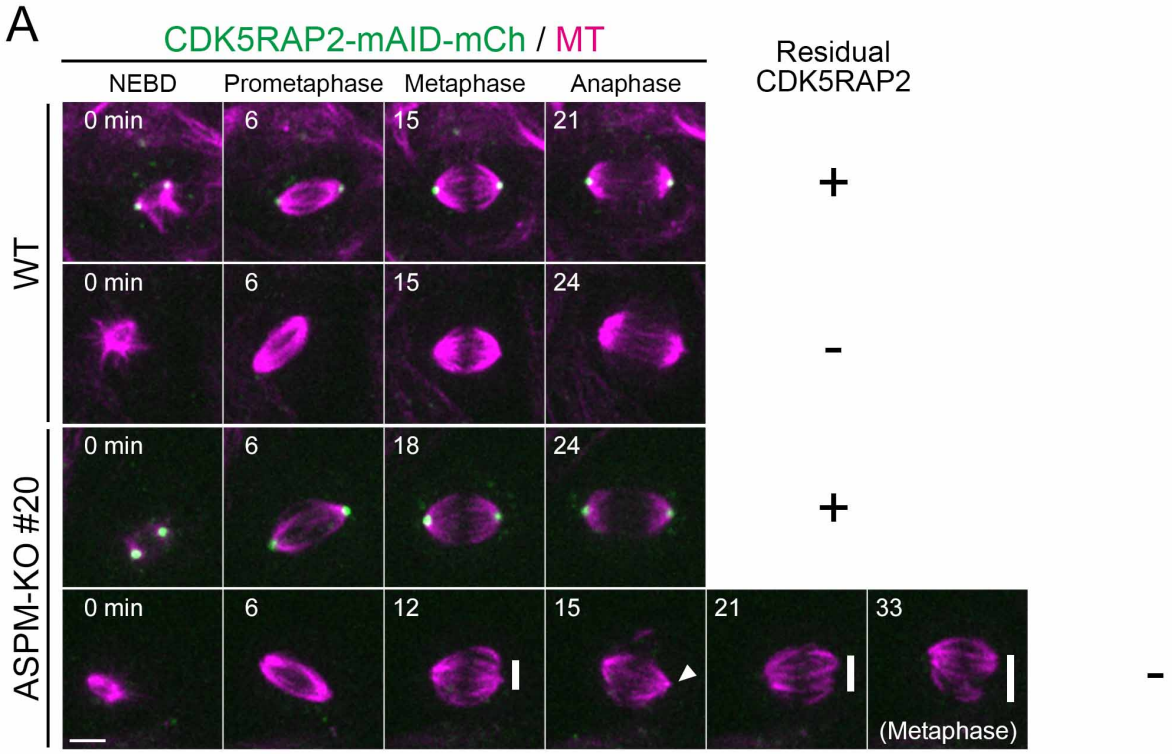

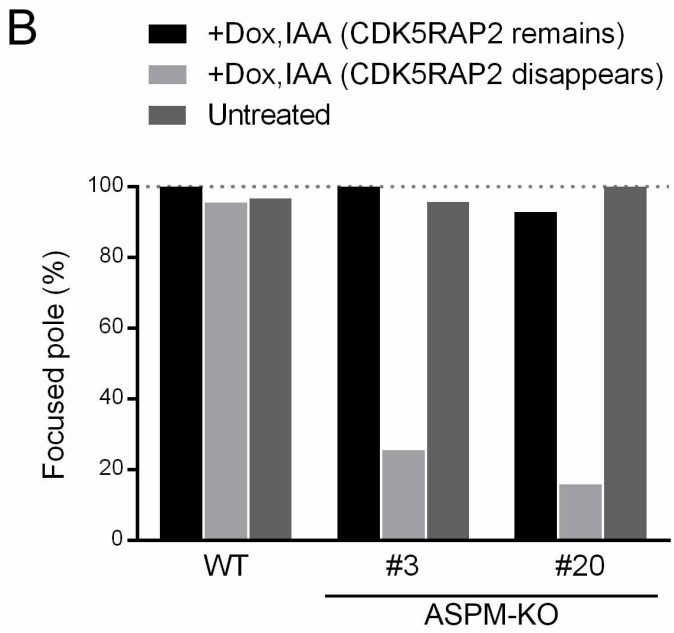

Figure 3. Spindle pole unfocusing upon double depletion of ASPM and CDK5RAP2
(A, B) Spindle pole unfocusing in the absence of ASPM and CDK5RAP2. Treatment with Dox and IAA induced the degradation of CDK5RAP2-mAID-mCherry (marked '–'). Cells that were tolerant to this treatment are also displayed as the control (marked '+'). Two independent KO lines (#3 and #20) were analysed. Arrowhead and vertical lines indicate focused and unfocused poles, respectively; pole focusing was observed only transiently. Images were acquired with 5 z-sections (separated by 3 μm) and displayed after maximum projection. See also Movie 3. Experiments were performed twice, and the result of one experiment is displayed in the graph (n = 8–44). Bar, 5 μm.

Figure 4

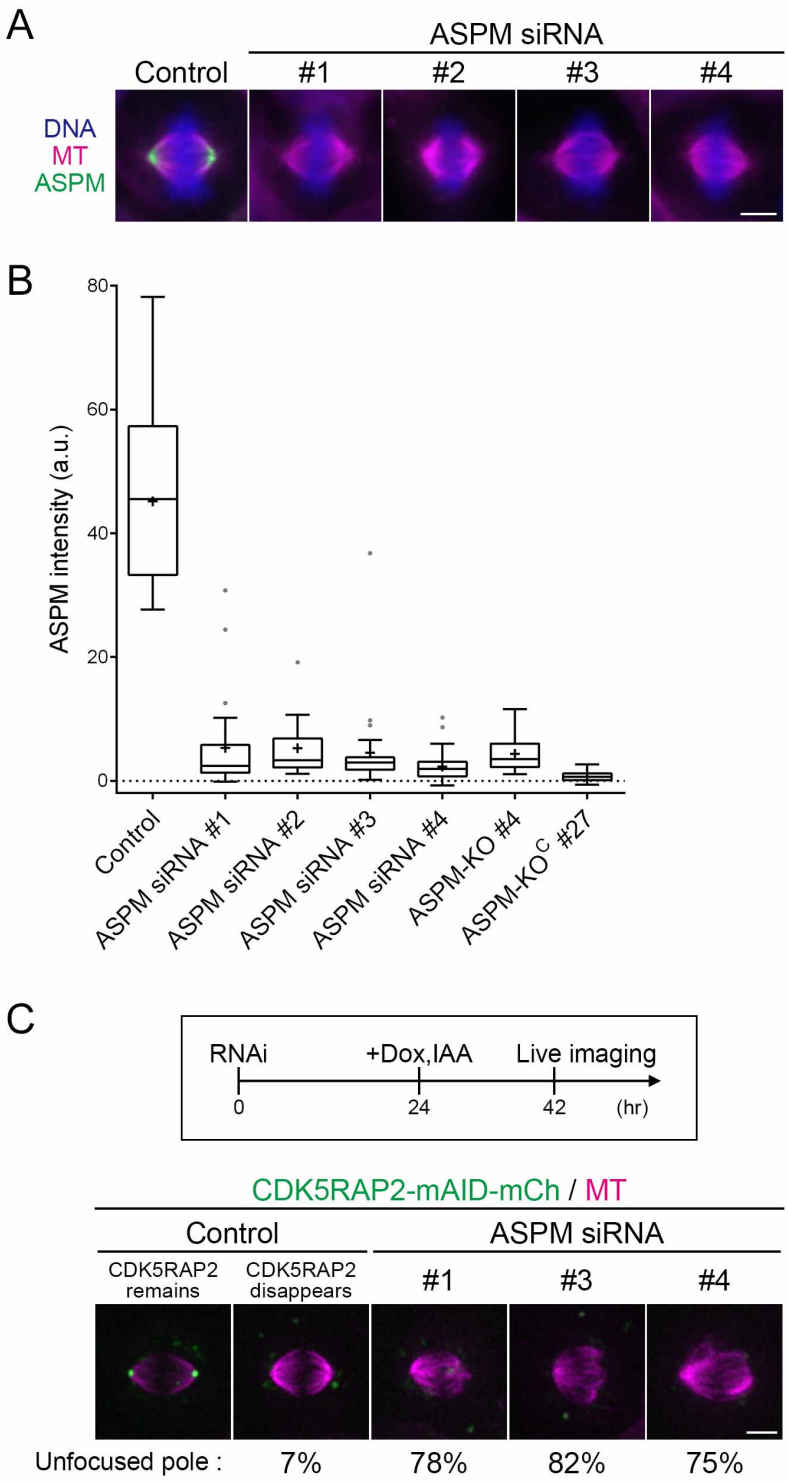

Figure 4. RNAi-mediated knockdown phenocopies KO
(A, B) Efficient knockdown of ASPM using four independent RNAi constructs as indicated by immunofluorescence microscopy (A) and the signal intensity measurement (B). The data are shown as a box-and-whisker plot, with the median (line in the middle of box), upper and lower quartiles (the ends of box), maximum and minimum (whiskers), outlier (dots), and mean (marked '+') values presented; n = 13–55. Experiments were performed twice, and the result from one experiment is displayed in the graph. **(C)** Spindle pole unfocusing by combined ASPM knockdown and CDK5RAP2 degradation. Two control images (± CDK5RAP2-mCherry signals) are also displayed. Images were acquired with 5 z-sections (separated by 3 μm) and displayed after maximum projection; n = 9–30. Experiments were performed twice, and the result from one experiment is displayed in the graph. Bars, 5 μm.

Figure 5

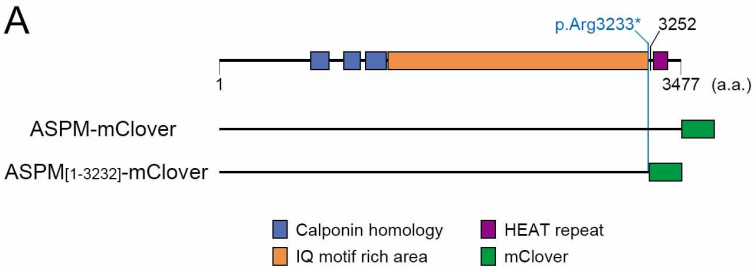

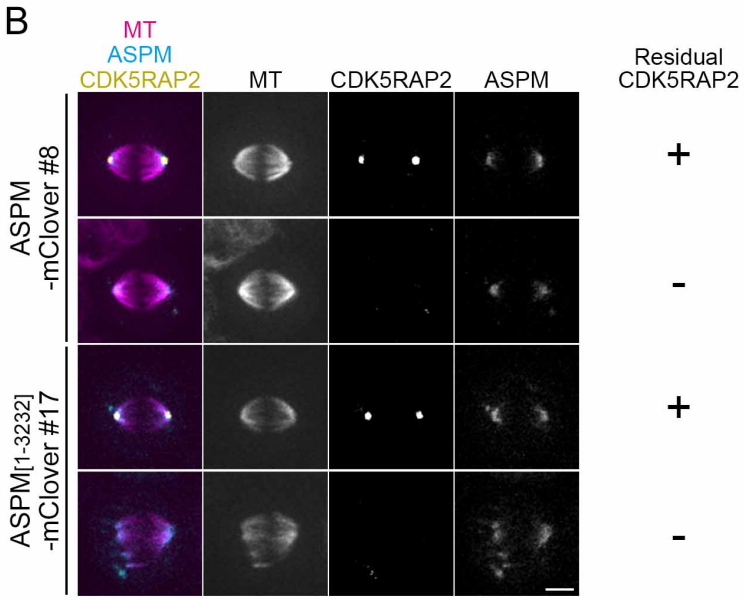

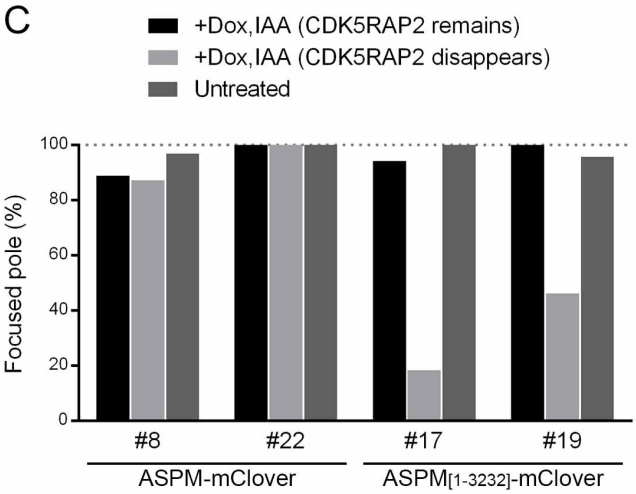

Figure 5. Hypomorphic microcephaly mutation impairs the spindle pole-focusing function of ASPM

(A) mClover insertion after the aa 3,232 residue mimics the second-most C-terminally truncated protein identified among the microcephaly patients (Abdel-Hamid et al., 2016; Bond et al., 2003; Tan et al., 2014). As a control, mClover was tagged to the C-terminus of the full-length ASPM protein. **(B, C)** Spindle pole unfocusing caused by ASPM truncation in the absence of CDK5RAP2. Treatment with Dox and IAA induced the degradation of CDK5RAP2-mAID-mCherry (marked '–'). Cells that were tolerant to this treatment are also displayed as the control (marked '+'). Two independent truncation lines (clones #17 and #19) and control full-length ASPM-mClover lines (clones #8 and #22) were analysed. See also Movie 4. Images were acquired with 5 z-sections (separated by 3 μm) and displayed after maximum projection. N = 9, 47, 31 (full-length #8); 12, 19, 33 (full-length #22); 17, 38, 15 (mutant #17); and 6, 26, 23 (mutant #19). Bar, 5 μm.

Supplemental figure 1 (A-D)

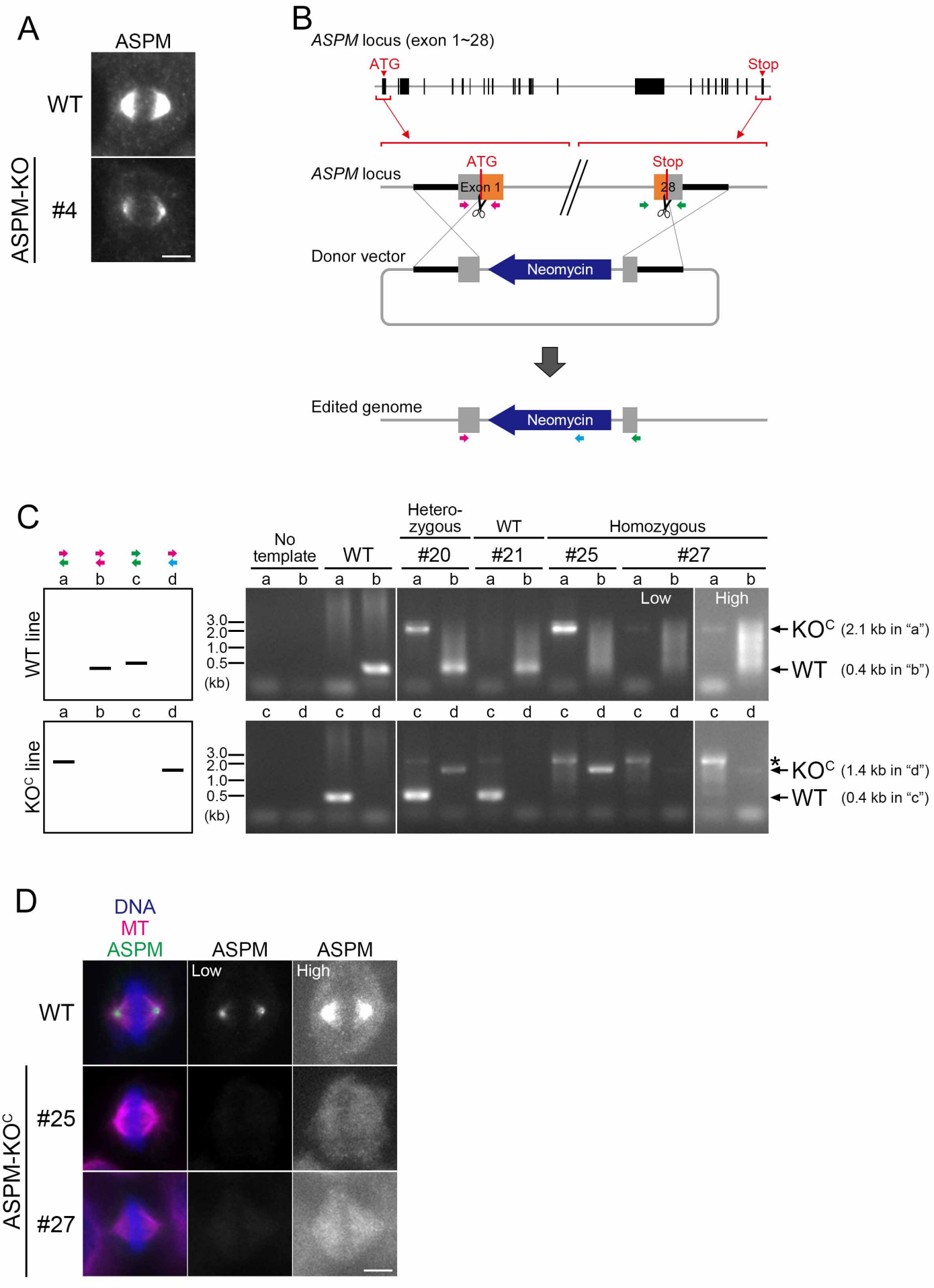

Supplemental figure 1 (E,F)

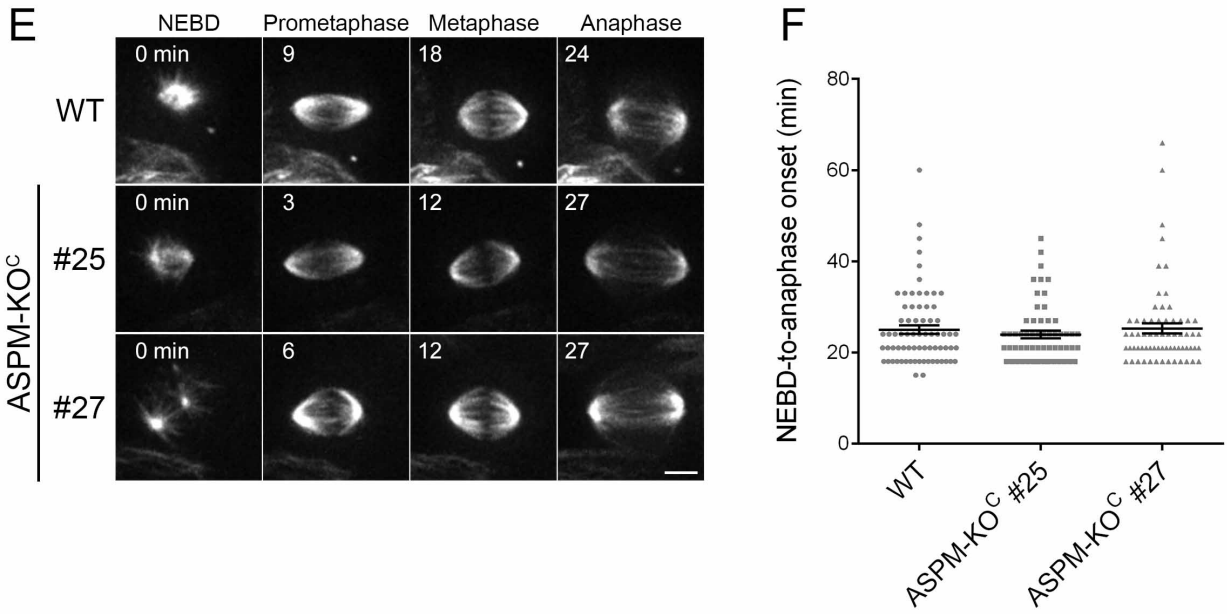

Figure S1. Construction of the complete ASPM KO line
(A) In *ASPM* KO cells for which exon 1 was targeted, truncated ASPM protein was still weakly expressed and detected at the spindle pole. Note that signals in this figure were highly enhanced to best visualize the weak signals in the KO line (identical cells to those in Fig. 1C are displayed). **(B, C)** Construction of the complete *ASPM* KO line (KOC), in which the entire *ASPM* open reading frame was replaced by the neomycin-resistant marker. Targeted integration of the marker cassette was confirmed by PCR (primers are indicated as arrows in B). Expected bands are displayed on the left of (C). Asterisk in (C) indicates a non-specific band. **(D)** Complete *ASPM* KO (KOC) lines did not give rise to pole staining with anti-ASPM antibody. Images with highly enhanced signals are presented on the right. **(E)** Spindle dynamics of *ASPM* KOC lines. MTs were visualized by SiR-tubulin staining. Images were acquired with 5 z-sections (separated by 3 μm) and displayed after maximum projection. No abnormality was detected. Images of two clones (#25 and #27) are shown. **(F)** Mitotic duration with or without ASPM. Data are mean ± SEM. WT; 25 ± 1 (n = 71), KO #25; 24 ± 1 (n = 59, $p > 0.4$, Student's t-test), KO #27; 25 ± 1 (n = 66, $p > 0.8$). Bars, 5 μm.

Supplemental figure 2

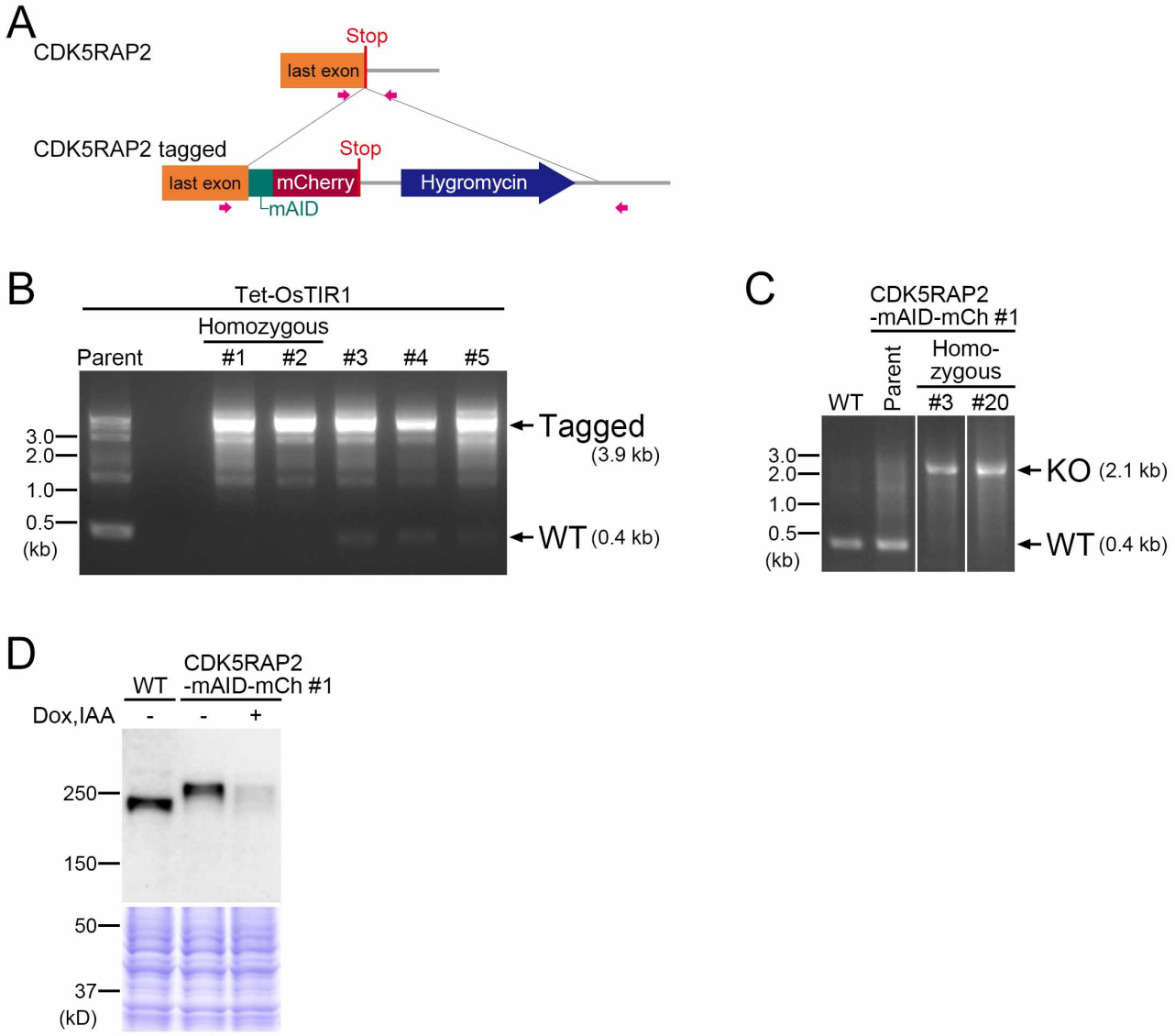

Figure S2. Construction of the CDK5RAP2-mAID-mCherry (degron) line
(A, B) Targeted integration of the marker cassette was confirmed by PCR (primers are indicated as magenta arrows). Clone #1 was used as the parent line of the following experiments. **(C)** ASPM was knocked out with the strategy described in Fig. 1A. **(D)** Confirmation of CDK5RAP2-mAID-mCherry protein degradation by Dox and IAA treatment. Immunoblotting using anti-CDK5RAP2 antibody and Coomassie staining of whole-cell extracts are presented. This blotting also confirmed the homozygous tagging of mAID-mCherry to CDK5RAP2.

Supplemental figure 3

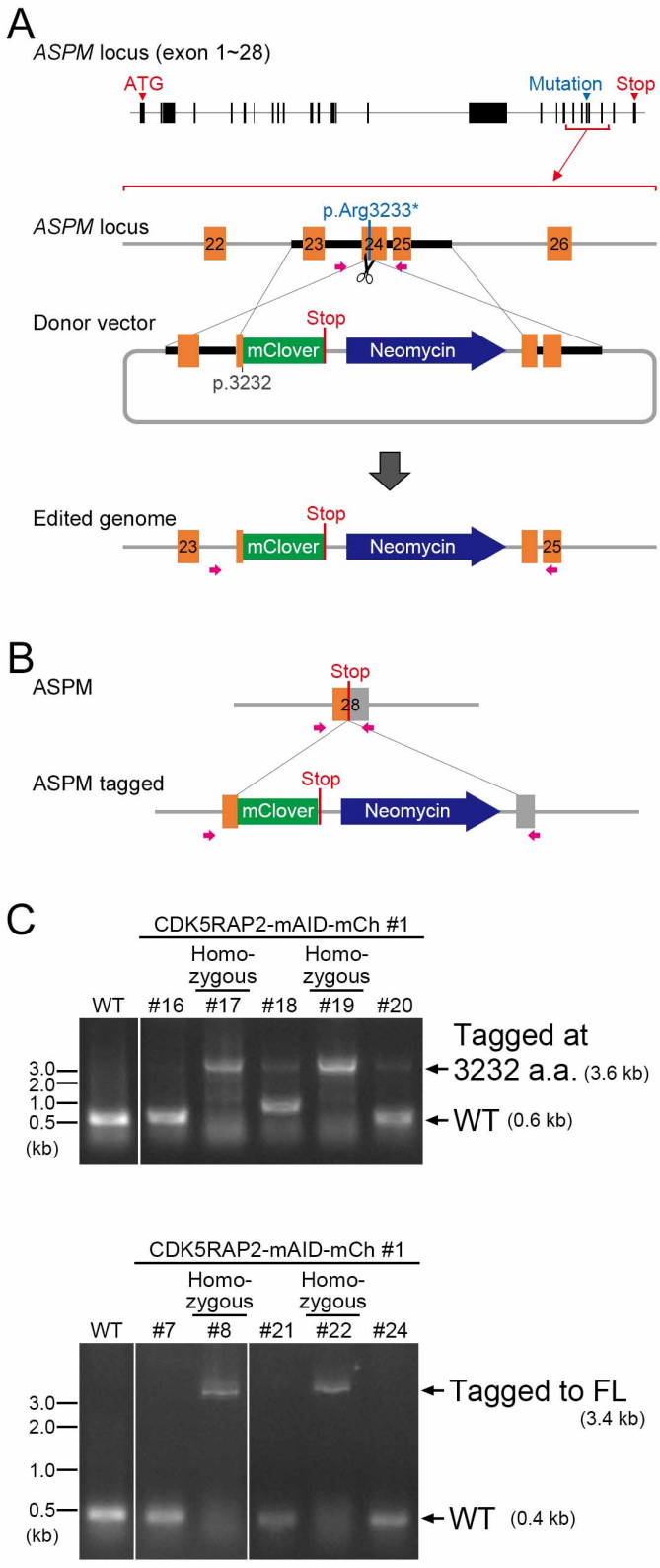

Figure S3. Construction of full-length and truncated ASPM-mClover lines
(A) Construction of the truncated ASPM line, in which mClover and the neomycin-resistant gene were inserted at exon 24, which mimicked the second-most C-terminally truncated protein identified among microcephaly patients (aa 1–3,232). **(B)** As a control, mClover and the marker were integrated at the C-terminus of the full-length ASPM protein. **(C)** Targeted integration of mClover and the marker cassette was confirmed by PCR (primers are indicated as magenta arrows in A and B). The CDK5RAP2-mAID-mCherry line (clone #1) was used as the host of integration. Proper tagging of mClover (ASPM-mClover #8 and #22, ASPM [1-3,232 a.a.]-mClover #17 and #19) was also verified by DNA sequencing after PCR.